Journal of Materials Chemistry B

Accepted Manuscript

ROYAL SOCIETY OF CHEMISTRY

www.rsc.org/materialsB

Discrimination between Bacterial Phenotypes using Glyco-Nanoparticles and the Impact of Polymer Coating on Detection Readouts

Sarah-Jane Richards,[a] Elizabeth Fullam,[b,c] Gurdyal Besra [b] and Matthew I. Gibson [a],*

[a] Department of Chemistry,

University of Warwick,

Coventry,

CV4 7AL

[b] School of Biosciences and Institute of Microbiology

University of Birmingham

[c] School of Life Sciences, University of Warwick

*Corresponding Author Information

Fax: +44(0)2476 524112;

E-mail : m.i.gibson@warwick.ac.uk

Abstract

The identification and treatment of bacterial infections remains a major healthcare challenge, especially to ensure appropriate application of a limited spectrum of antibiotics. Here we describe a system capable of discriminating between different strains of *Escherichia coli* using multivalent, carbohydrate-functionalised, gold nanoparticles based on their different expression levels of the FimH adhesin. Upon binding of the glycosylated nanoparticles to FimH positive bacteria, the nanoparticles' optical properties change enabling the identification of bacteria strain. Comparison between direct conjugation, or *via* a linker, of the carbohydrate to the nanoparticle revealed significant effects on the performance of the detection system. Using a poly(ethylene glycol) spacer increased the stability, and specificity, of the glycosylated nanoparticles but also reduced aggregation upon bacterial binding. This prevented the well-know red-blue gold colour change, meaning spectrophometric, rather than optical, assessment methods were required. Using this method, FimH positive bacteria could be detected at approximately 1.5 $x10^7$ colony forming units/mL.

Introduction

Due to their widespread overuse, and the emergence of resistance, antibiotics are becoming less effective and agents that were once last resort are now being used more frequently. This has lead to a looming major healthcare crisis, with few new antibiotics in the pipeline, new strategies to treat and identify bacterial infections are urgently required.[1, 2] Standard clinical methods for the detection and identification of bacterial pathogens such as *E. coli*, rely upon selective conventional culturing and plating of bacteria from a contaminated sample and conclusive results typically require 24 hours or more. Despite being sensitive and accurate, it does not provide real-time, on-site feedback and requires sophisticated equipment and often immunoassays using fluorescence or radiolabelling.[3-5] A direct, label-free method for bioanalyte detection that is easy, sensitive even at low sample volume, high-throughput and quantifiable in real-time is critical to applications in clinical diagnostics and the real-time detection of environmental and biological toxins.[6]

Goldnanoparticles (AuNPs) have been intensively studied in bioanalytical applications due to their characteristic optical properties. They are also good alternatives to fluorescently or radiolabelled substrates used in bioassays because they are inexpensive, simple to synthesise, have high photo-stability and can be conjugated efficiently to biological molecules.[6, 7] AuNPs exhibit an intense colour in the visible region due to a local surface plasmon resonance (LSPR) which arises due to the collective oscillation of the conduction-band electrons of the gold core.[6, 8-10] These optical properties are strongly correlated with their size, shape, dispersion media and degree of aggregation making them ideal sensors. Aggregation of AuNPs leads to a dramatic colour change from red to blue/purple. This is due to electric dipole-dipole interactions and coupling between the plasmons of neighbouring particles.[6, 8-10]

Triggered changes in their aggregation can be readily observed by eye and quantitative analysis only requires a UV-Vis spectrometer. It is for this reason that AuNPs are attractive for the detection of biomolecules.[8, 11] The colour changes associated with AuNP aggregation have been exploited in the development of colourimetric assays using AuNPs functionalised with biomolecules such as proteins,[7, 12] peptides,[11] antibodies[13-18] and DNA.[19, 20] The detection of bacterial DNA using AuNPs originated in the pioneering work of Mirkin *et al.*,[20] who demonstrated that as little as 10 fmol of an oligonucleotide analyte could be detected by exploiting the aggregation phenomenon of AuNPs. Many groups have used AuNP-based sensors in an immunoassay format, whereby disease markers can be detected using AuNPs conjugated to appropriate antibodies.[12, 14, 16, 17] The *in situ* generation of gold nanoparticles guided by enzymes has also been exploited to create ultra sensitive sensors for the detection of prostate cancer and HIV antigen p24.[21] Rotello *et al.* have developed gold nanoparticle sensors, whereby bacteria adhesion to the nanoparticles releases β-galactosidase from the surface, activating a pro-fluorescent label, providing detection of the presence of bacteria, but not the phenotype.[22]

Protein-carbohydrate interactions mediate many critical biological recognition processes, such as those involved in cell signalling, fertilisation, and inflammation, and in particular, they mediate the adhesion of viruses and bacterial toxins to their native targets.[23, 24] The proteins responsible for deciphering this information are termed lectins, which specifically (and noncovalently) bind carbohydrates.[25, 26] The protein–saccharide interactions are usually weak, but are amplified by clustered saccharides, resulting in a binding constant, which is greater than the simple sum of the total number of ligands. This observation is referred to as the "cluster glycoside" effect.[27, 28] Considering this information, carbohydrate functionalised AuNPs

(glycoAuNPs) are attractive biosensors as they are inherently multivalent and should give optical responses upon protein binding to their surface, providing the platform for new sensors.[8, 10, 29] There have been many reports of using mannose or glucose functional AuNPs to interact with Concanavalin A (ConA) as a model protein.[8-10, 29-32] ConA, however, is not an indicated target for biosensing. A more relevant target for carbohydrate-based bioanalytical platforms are outer membrane-exposed lectins on the surface of bacteria (or indeed viruses), which are involved in cellular adhesion to the glycocalyx of mammalian cells.[33, 34] One of the most important and most investigated bacterial lectins is the mannose/glucose-specific protein FimH, which is expressed on the tips of Type 1 fimbriae on *E. coli*. These fimbriae are uniformly distributed on Enterobacteriaceae, commonly between 100 and 400 fimbriae per cell.[34] Alexander and coworkers have employed thermoresponsive glycopolymers to reversibly aggregate FimH expressing bacteria upon changing the external temperature.[35] Disney *et al*. used fluorescent glycopolymers to detect FimH positive bacteria, but this required an isolation step limiting the sensory application.[4] Gold nanoparticles have been reported to bind to fimbriae, but identification was achieved *via* electron microscopy, and not exploited their colorimetric properties.[31] The colourimetric (red-blue) shift associated with gold nanoparticle aggregation has been exploited for the detection of isolated lectins, and different strains of influenza[36] but not to identify bacterial phenotype.

In this work we investigate the development of a colourimetric glyconanoparticle assay for the rapid, point-of-care, detection of particular bacteria phenotypes based on their surface lectin expression patterns. The role of particle structure including polymeric spacer on the sensitivity, specificity and outputted signal is investigated.

Results and Discussion

In order to obtain glycosylated nanoparticles which could selectively interact with the FimH adhesin on *E. coli*, gold nanoparticles were synthesised using the one-pot method of Watanabe *et al.*,[8] using chemical reduction of $HAuCl_4$ using a thio-sugar as the reducing and stabilising agent. Different sized particles were obtained by tuning the molar ratio of thioglucose:Au^{3+}, Scheme 1. Although glucose is not the native ligand for FimH (mannose), there are several reports of multivalent glucose binding FimH so was a suitable starting point.[35] Table 1 summarises the initial particles used in this study. By varying the ratio of thioglucose relative to Au^{3+} it was possible to control the diameter of the gold nanoparticles in the range of 30 – 60 nm, as confirmed by UV-Vis and dynamic light scattering (DLS).

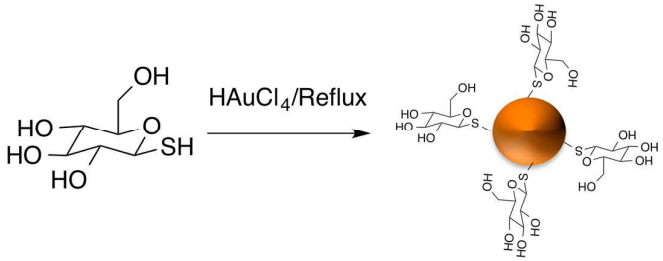

Scheme 1. Synthesis of gold nanoparticles by *in situ* reduction using 1-thioglucose

Table 1. Gold nanoparticles synthesised by *in situ* reduction

Code	Molar ratio Thioglucose:Au^{3+}	Wavelength of SPR peak (nm)	Diameter[37] (nm)
AuNP1	0.55	525	32
AuNP2	0.50	530	48
AuNP3	0.45	536	60

To probe the utility of the glyconanoparticles as colourimetric readouts of the presence of lectins, ConA was selected due to its well-known affinity for glucose/mannose residues. During the initial experiments, it became clear that the glyconanoparticles could not tolerate significant quantities of salt in the buffer, so the

NaCl concentration had to be reduced (see below for solutions to this – it is crucial for point-of-care diagnostics) to prevent unwanted aggregation. Addition of ConA to the nanoparticles resulted in a shift in the location of the SPR peak to longer wavelengths (i.e. blue colouration) and a general increase in absorption at 700 nm, Figure 1. By plotting Abs_{700} against ConA concentration, it was possible to obtain binding isotherms that indicated larger nanoparticles had increased affinity to ConA, compared to the smaller ones. However, unravelling relative affinity/avidity in multivalent systems is non-trivial,[38, 39] and the experiments shown here simply serve to demonstrate that the response of the AuNPs to ConA has a size dependency. To probe the underlying mechanism of this shift in the absorption behaviour of the gold, the process was monitored kinetically, by both UV-Vis and DLS, Figure 1C. The increase in diameter observed by DLS correlated well with Abs_{700} confirming that lectin/nanoparticle crosslinking was the macroscopic effect. This observation is crucial if a red-blue colour shift is to be obtained. If lectin adhesion does not lead to particle crosslinking the spectral changes would be more subtle and require different analysis, and is described later.

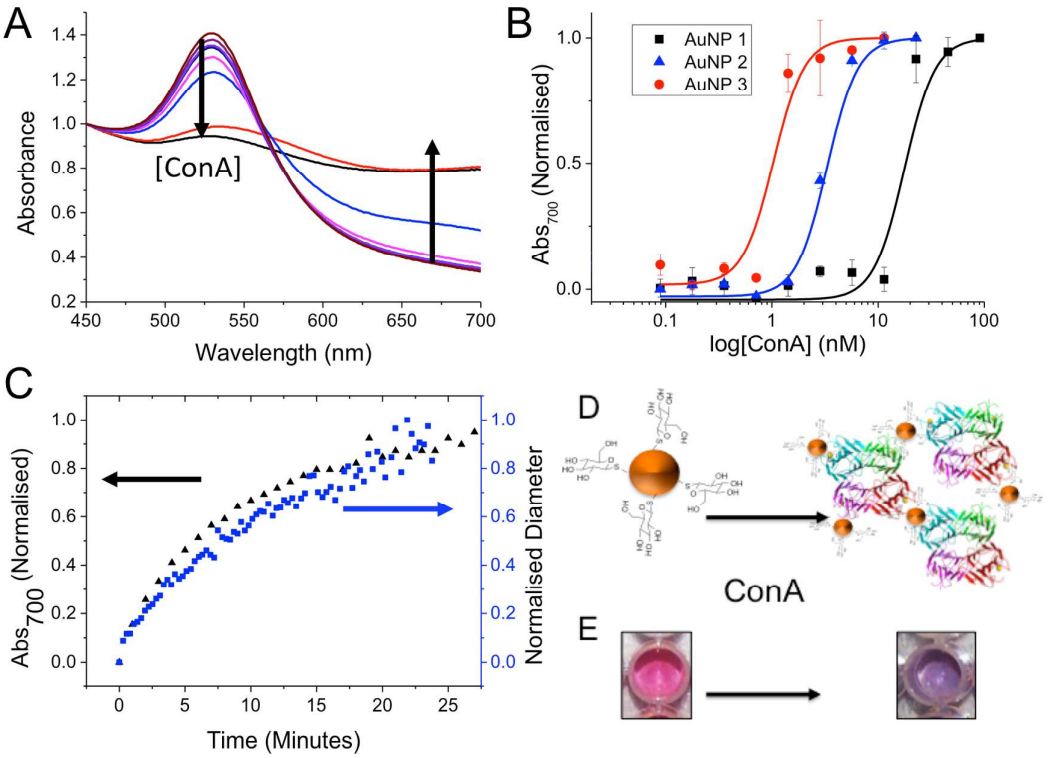

Figure 1. Interaction of glucose-functional glyconanoparticles with ConA. A) UV-Vis spectrum of **AuNP2** upon addition of increasing concentrations of ConA (0.1 – 100 nM) following 30 minutes of incubation; B) Binding isotherms (at 37 °C) of glyconanoparticles with ConA; C) Comparison of kinetics of nanoparticle responses to ConA by both UV-Vis spectroscopy and dynamic light scattering; D) aggregation of gold nanoparticles by ConA tetramer giving rise to colour changes (E).

Encouraged by the colour shift in response to addition of ConA, **AuNP2** was selected to interrogate two distinct strains of *E. coli*; K-12 (strain K-12 JM109) which expresses FimH, mannose-binding adhesin on its fimbriae; TOP10, which does not express FimH. The nanoparticles were incubated with a dilution series of each bacteria in a range of ODs (Optical Density – bacteria density in solution by measuring absorbance at 600 nm) from 0 to 1, for 30 minutes and their absorption spectra recorded, Figure 2. As can be clearly seen in Figure 2A, addition of **AuNP2** to

K-12 resulted in a large shift in the SPR maximum to longer wavelength and an increase in absorbance at 700 nm (after correcting for the background absorbance of the bacteria), in agreement to what was observed with ConA. With TOP10 (no FimH), the observed changes were smaller, and only occurred at higher bacteria concentrations, indicating either non-specific (fouling) interactions or unintended interactions with unknown proteins such as glucose transporters. Figure 2C shows the binding isotherm, which shows the particles responded to the K-12's at far lower concentration (100 fold) than the TOP10's, demonstrating in principle the nanoparticle's ability to discriminate. Figure 2D shows photographs of the nanoparticles with bacteria showing the very obvious colour changes from red-blue in the presence of K-12s, but not with TOP10 until very large concentrations are applied which could form the basis of a point of care diagnostic if selectivity could be improved. This limited range of selectivity is probably due to the earlier observations that the gold nanoparticles have limited stability in complex media (and saline) and hence some aggregation will occur over time giving false-positive readouts.

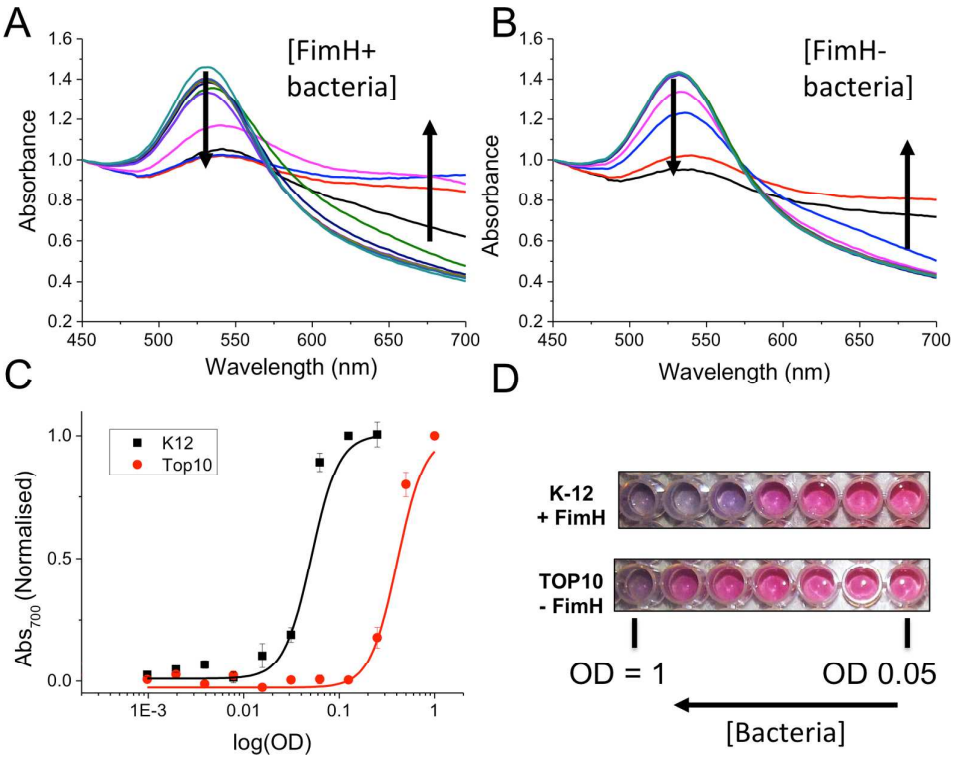

Figure 2. Interactions of **AuNP2** with K-12 and TOP10 bacteria. A) Absorption spectra of **AuNP2** upon addition of K-12 bacteria of OD 0.001 to 1; B) Absorption spectra of **AuNP2** upon addition of TOP10 bacteria of OD 0.001 to 1; C) Comparison of binding isotherm of glycoparticles to both bacteria at 37 °C; D) Photographs of **AuNP2** with serial dilution of bacteria and associated colour changes.

Encouraged by the results described above, a strategy was developed to improve the selectivity and stability of the nanoparticles. To improve solution stability, it is common to immobilise hydrophilic 'non-fouling' polymers which confer both saline stability and reduce non-specific absorption of proteins onto the nanoparticle surface, most commonly with poly(ethyleneglycol) (PEG).[40] Furthermore, to improve binding to FimH, mannose was selected as the more specific ligand, compared to glucose. Installation of the mannose onto thiol-terminated PEG was achieved by cycloaddition of α-D-propargyl mannoside with the ω-terminal azide ('click'), followed by

purification by dialysis, Scheme 2. The mannose-functional PEG was subsequently immobilised onto pre-formed 40 nm nanoparticles by a simple mixing strategy and excess polymer removed by centrifugal dialysis. Upon polymer coating an increase in hydrodynamic diameter from 40 – 55 or 57 nm was observed, along with a shift in the SPR_{max} indicating successful functionalisation, Table 2.

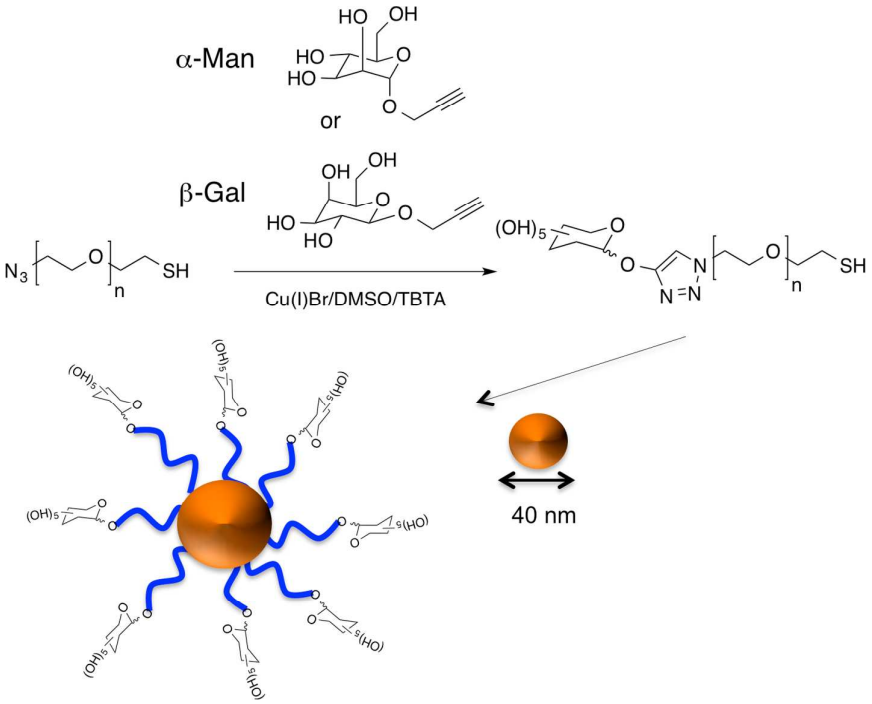

Scheme 2. Synthesis of PEGylated glyconanoparticles

Table 2. Glyconanoparticles with PEG spacer

Code	Carbohydrate	$SPR_{uncoated}$[(a)] (nm)	SPR_{PEG}[(b)] (nm)	Diameter[(c)] (nm)
NP-Man	α-Man	525	527	55
NP-Gal	β-Gal	525	529	57

(a) SPR maximum of 40 nm uncoated gold nanoparticles; (b) SPR maximum of gold nanoparticles after coating with pyranoside-PEG-SH; (c) Diameter determined by DLS

As saline stability was a problem with the directly carbohydrate-conjugated gold nanoparticles, resulting in false positive aggregation effects, the stabilising effect of the PEG was assessed, Figure 3. The PEGylated nanoparticles were stable across all NaCl concentration ranges (up to 1 M, which is above that required for a sensor) whereas the non-PEGylated particle aggregated even at 0.005 M NaCl. This assay ensures that any aggregation effects observed with live bacteria can be assigned to particle-bacteria interactions and not to non-specific aggregation.

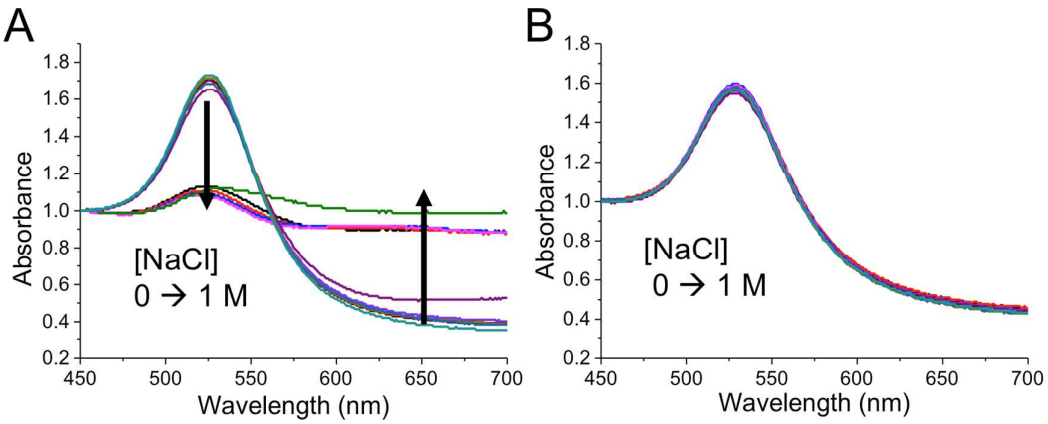

Figure 3. Comparison of saline stability of (A) uncoated and (B) PEG-coated nanoparticles.

As with **AuNP 1-3**, ConA was added to the particles and their responses measured by UV-Vis. Unlike the previous examples, addition of ConA did not appear to cause a shift in the SPR maximum, but did induce a large increase at 700 nm, and a decrease in intensity of the SPR peak, Figure 4. Kinetic analysis (at Abs_{700}) showed the rate of change in absorbance for the PEGylated particles was significantly slower than with **AuNP2**. **AuNP2** aggregated in less than 25 minutes, but the PEGylated particles were still increasing at 700 nm even after 4.5 hours of incubation. This is interpreted as being due to the increased stability of the PEGylated particles in the buffer, which means there are no non-specific aggregation events. The increased separation between

carbohydrate residues at the termini of PEG-chains (relative to directly-conjugation to gold surface) may also slow the rate of binding due to spacing effects.

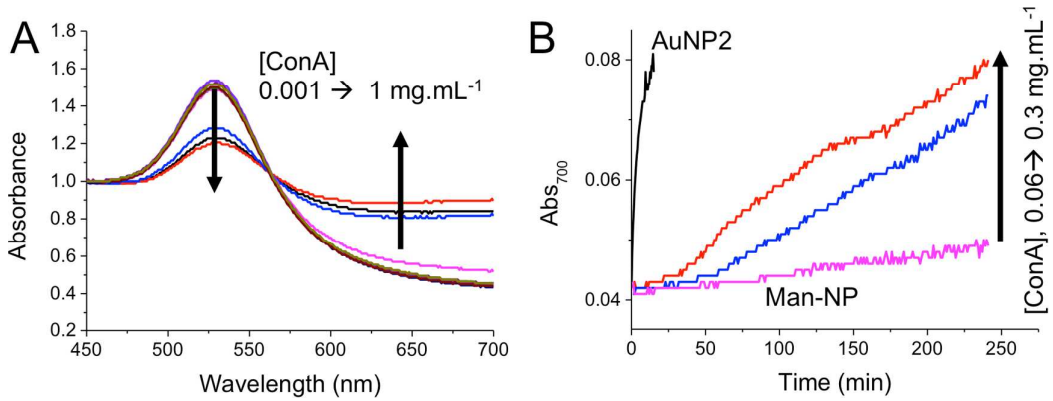

Figure 4. Interactions of **NP-Man** with ConA. A) Absorption spectra of particles upon addition of ConA at 37 °C for 30 minutes; B) Kinetic analysis of nanoparticle interaction with ConA, compared to non-PEGylated glyconanoparticle, AuNP2.

To unravel the processes that occur with both types of glyconanoparticle, and to aid the development of the optimum readouts for a sensor, the responses of AuNP2 and **NP-Man** are compared in Figure 5. The change in absorption at 700 nm (after 30 minutes) for both nanoparticles as a function of ConA concentration is almost identical, with similar inflection points. However, the changes in the SPR absorption band are in stark contrast. AuNP shows a dose–dependent shift in SPR_{max} as [ConA] increases. **NP-Man** however, does not show any shift in the SPR and hence there is no red-blue colour shift, suggesting more analysis is required if there are to be used as a diagnostic tool. DLS analysis (Supp Info) showed no aggregation of **NP-Man** upon addition of ConA. We therefore propose that the SPR shift (red – blue) seen for AuNP1-3 is associated with the interparticle distance decreasing, due to ConA crosslinking the particles or due to binding events leading to reduced solution

stability. The change in absorption at 700 nm for **NP-Man** is not a turbidity effect (due to no increase in particle diameter for PEGylated particles) and we therefore suggest this is associated with protein binding to the nanoparticles and affecting their hydration, and hence refractive index. These observations raise a question for the use of gold particles as biosensors, in that the commonly applied polymer coatings improve stability, but inhibit the convenient visual read-out commonly associated with nano-gold red-blue colour shift. Therefore, absorption at 700 nm will be used from this point. It should be noted that the effect of polymer coating will vary on the analyte being detected (including size of analyte: e.g. bacteria/virus), and the length of the polymer itself.[36]

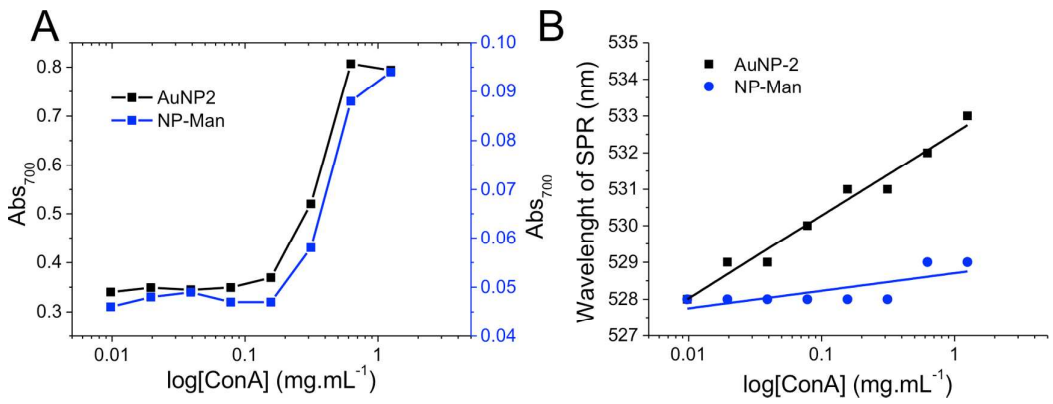

Figure 5. Comparison of spectral response between particles with and without PEG spacer. A) Change in absorbance at 700 nm; B) Changes in the location of the SPR absorption band as a function of lectin concentration.

Before progressing to testing with the bacteria, an additional control experiment was undertaken. Peanut agglutinin (PNA), which has preference for β-galactose was added to **NP-Man**. Pleasingly, no change was observed indicating that the polymer coating

efficiently prevents non-specific interactions with proteins, and only the carbohydrate motifs are associated with recognition/output events, Figure 6.

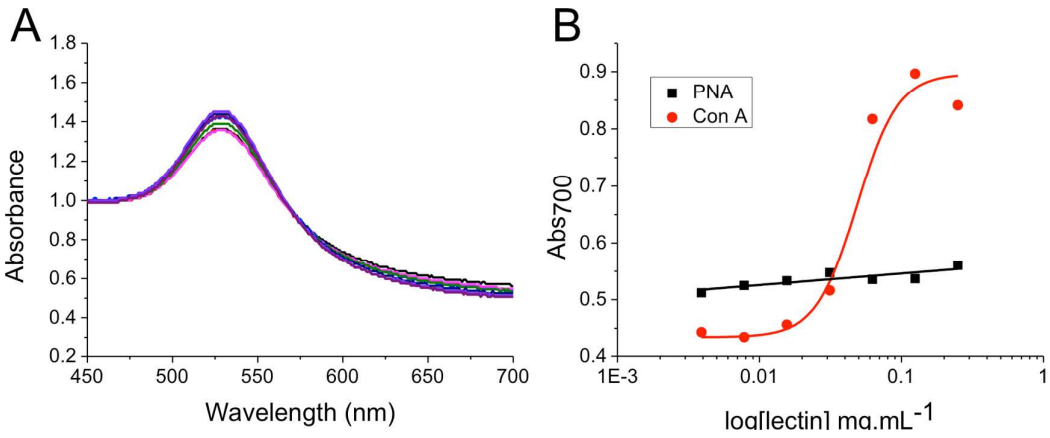

Figure 6. Assessment of lectin specificity of glyconanoparticles. A) UV-Vis spectra of **NP-Man** upon addition of PNA (0.001 – 1 mg.mL^{-1}); B) Comparison of change absorbance at 700 nm of **NP-Man** upon addition of ConA (mannose binding) and PNA (galactose binding).

With the above information in hand, a series of experiments were designed to probe bacterial specificity and the optical responses of the nanoparticles. To provide a negative control, galactose functional nanoparticles were also synthesised by identical synthetic methods, **NP-Gal**. **NP-Gal** should not interact with either of the bacterial strains, whereas **NP-Man** should interact with K-12 (the FimH adhesin) but not TOP10, and therefore providing a rigorous panel of measurements to probe sensitivity and selectivity. Figure 7 shows the UV-Vis spectra of **NP-Man** with K-12 and TOP10. As was observed with the protein studies, there was no shift in the SPR maximum with either bacteria but there were decreases in the SPR intensity and increases in absorbance at 700 nm. The changes observed were far more significant, and occurred at lower bacteria concentrations in the case of K-12 compared for

TOP10. The changes observed when **NP-Gal** was added to both bacterial strains was significantly less (Supp Info).

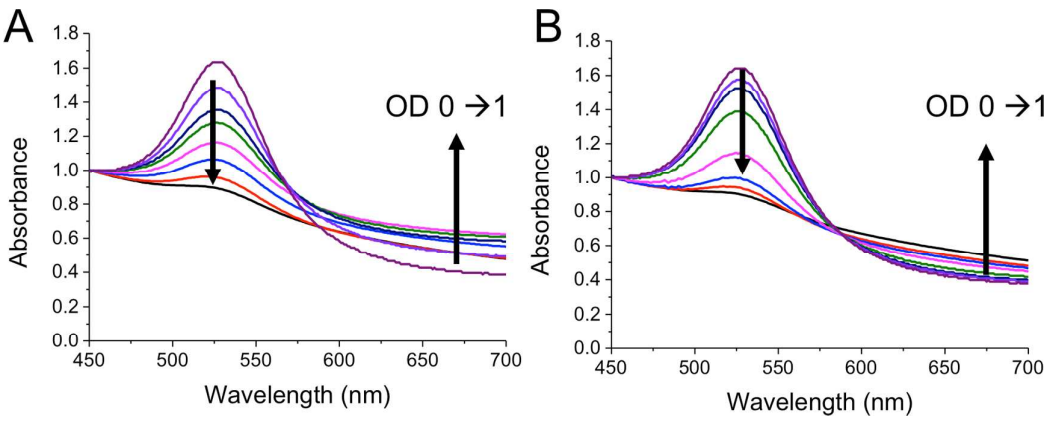

Figure 7. UV-visible spectra of **NP-Man** with K-12 (A) and TOP10 (B) bacteria.

The changes in absorbance at 700 nm for each bacterium at a variety of optical densities (proportional to bacteria concentration), with both particles is summarised in Figure 8. To aid visualisation, the change in Abs_{700} as a function of OD was plotted as a heat map, with the z-axis (colour) set to show large changes as blue, and small changes as red (allowing facile comparison with standard nano-gold assays). Using this visualisation, it became very obvious that only Mannose-functional particles and K-12 together gave rise to positive responses. Changing to either TOP10 or Gal functional particles did not result in positive responses. The best responses were obtained with intermediate concentration of K-12, OD = 0.03 to 0.125 where the response to K-12 was largest without any response to TOP10. Very high concentrations of K-12 (> OD 0.5) actually led to a reduction in signal from **NP-Man**. We hypothesise that this is due to the bacteria binding sites saturating the gold particles, such that there are insufficient particles to statistically bind close together,

to give the desired optical outputs. Future studies will investigate this in more detail. The actual number of bacteria (colony forming units) was estimated (Supp. Info.) indicated that the nanoparticle system could detect K-12 bacteria at concentrations as low as 1.5 x 10^7 CFU/mL. These tests shows that glycosylated nanoparticles can discriminate between strains of bacteria based solely upon interrogation of membrane-exposed carbohydrate-binding proteins and could form the basis of new point-of-care diagnostics.

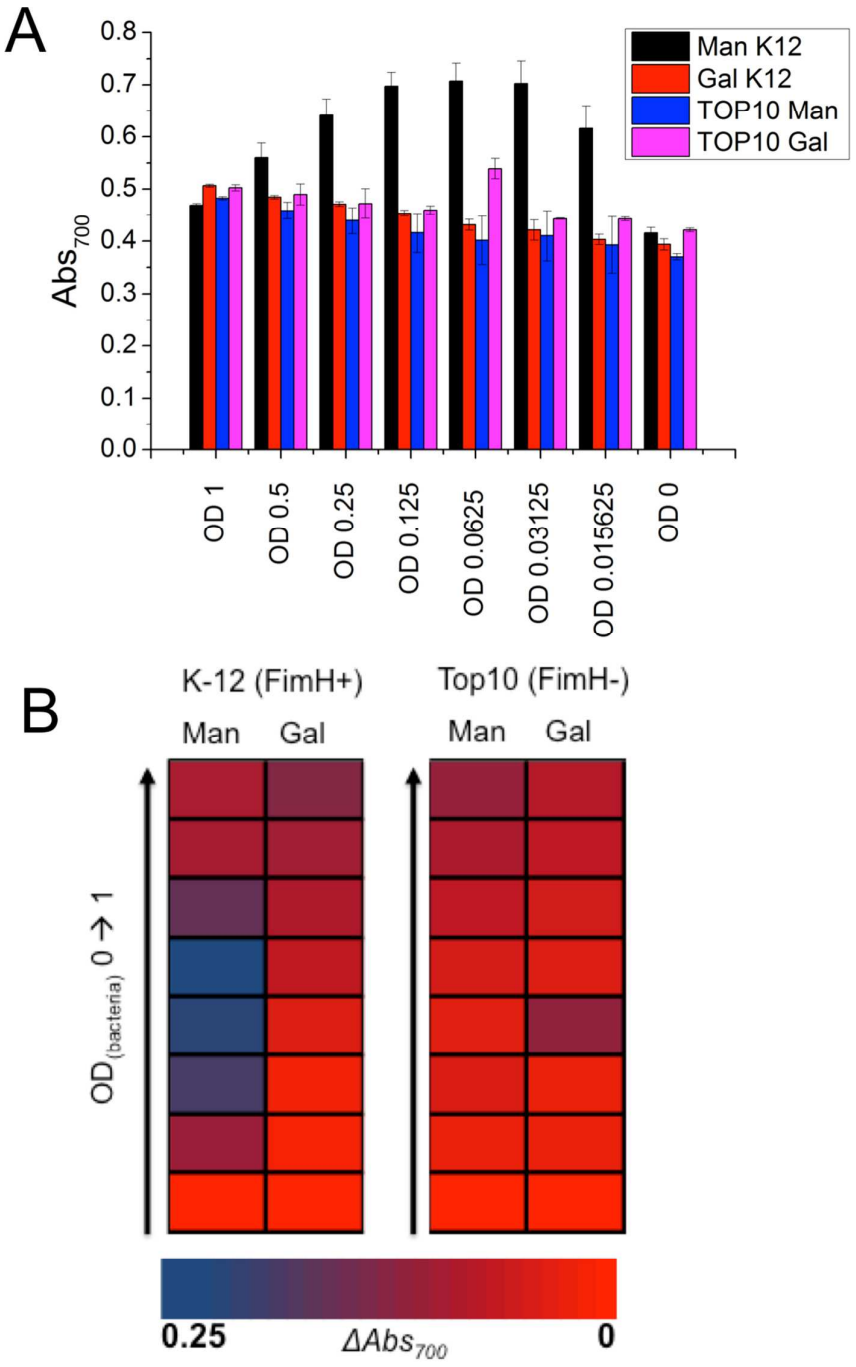

Figure 8. Responses of both **NP-Man** and **NP-Gal** to both K-12 and TOP10 bacteria. A) Absorbance at 700 nm for each system in response to bacteria, following subtraction of background absorbance of bacteria; B) Heat map showing change in Abs_{700} (relative to $OD_{bacteria}$ = 0) for all particles. Blue colouration indicates a larger

response and red indicates no response. Error bars indicate ± standard deviation from 3 experiments.

Conclusions

We have developed a sensitive and rapid colourimetric bioassay for the quantitative detection of lectins and Type 1 fimbriated bacteria based upon the binding of glycosylated gold nanoparticles. Gold nanoparticles with carbohydrates directly immobilised on their surface showed very rapid responses to both lectins and lectin-expressing bacteria. However, these particles also displayed low saline stability and nonspecific interactions with the bacteria limiting their discriminatory capacity. To overcome this a PEG layer was inserted between the particles and the carbohydrate. This dramatically increased the saline stability of particles whilst retaining their bio-recognition properties. An interesting side effect of the PEG layer was no red-blue colour change was observed upon lectin binding, which was hypothesised to be due to steric shieling effects of the PEG layer. Despite this, an assay was developed based on monitoring the absorbance at 700 nm with UV-Vis spectroscopy in which the mannose-functional particles specificity generated an output in the presence of K-12 bacteria and not TOP10. K-12 expressed type 1 fimbriae that bind mannose residues, but TOP10 does not. This system represents the first step in making nanoparticles that can ‘read’ the surface lectin composition of bacteria to enable rapid (point-of-care) phenotyping with a visual output.

Acknowledgements

Equipment used was supported by the Innovative Uses for Advanced Materials in the Modern World (AM2), with support from Advantage West Midlands (AWM) and part funded by the European Regional Development Fund (ERDF). MIG was a Birmingham Science City Interdisciplinary Research Fellow funded by the Higher Education Funding Council for England (HEFCE). SJR acknowledges the EPSRC MOAC doctoral training centre for a studentship. ECF is a Leverhulme Trust Early Career Fellow. G. B. is the Bardrick professor of microbial physiology and chemistry and holds a Royal Society Wolfson merit award.

Experimental Section

General

D-(+)-mannose, propargyl alcohol (99 %), copper bromide (99%), HEPES and phosphate buffered saline (PBS) were purchased from Sigma Aldrich. Triethylamine (99 %) and Hydrogen tetrachloroaurate (III) trihydrate were purchased from Acros. β-D-thioglucose sodium salt was purchased from Carbosynth. D-(+)-galactose anhydrous was purchased from MP Biomedicals. DMSO was purchased from Fisher Scientific at laboratory grade. Peanut Agglutinin and Concanavalin A were purchased from Vector Laboratories. Azido PEG thiol (N_3-(PEG)-SH, Mn = 3000 $g.mol^{-1}$) was purchased from NANOCS. Tris-(benzyltriazolylmethyl)amine (TBTA) was synthesised according to literature procedures.[41] Microtitre plates were purchased from Greiner Bio-one. 10 mmol HEPES buffer containing 0.15M NaCl, 0.1mM $CaCl_2$ and 0.01mM Mn^{2+} (pH 7.5, HEPES) was prepared in 200 mL of milliQ water (with a resistance >19 mOhms). 40 nm gold nanoparticles were obtained from BBI International. K12 JM109 (referred to as K12 in text) and TOP10 were both grown in LB media from frozen stocks prior to use. Bacteria were isolated by centrifugation and the resuspended to the desired optical densities in PBS.

Instrumental

Absorbance measurements of the nanoparticles incubated with ConA were recorded on a BioTek SynergyTM HT multi-detection microplate reader obtained using Gen5 1.11 multiple data collection and analysis software. DLS measurement were carried out using a Malvern Instruments Zetasizer Nano-ZS. A Thermoscientific NanoDrop 2000 UV-Vis Spectrophotomer was used to measure the OD_{600} of the *E. coli* cells.

Synthesis of Glucose Functionalised Gold Nanoparticles

Thioglucose-capped gold nanoparticles were synthesized according to the method of Wantanabe *et al.*[8] An aqueous 1-thioglucose solution (5.0 mL 2-20 nM) was added to a boiling solution of $HAuCl_4$ (50 mL, 0.5 mM) under reflux and vigorous stirring. On addition of the 1-thioglucose, the solution changed colour from pale yellow to ruby red almost immediately. Then the reaction was heated under reflux for a further 10 minutes. The reaction mixture was cooled and dialysed overnight against water to remove unreacted thioglucose using dialysis tubing (Spectra/Por, Cellulose ester, MWCO = 5000, Spectrum Laboratories Inc., USA).

Synthesis of Propargyl-Pyrannosides

To mannose or galactose (500 mg,) in propargyl alcohol (5 mL), 250 µL of 3 M HCl was added. Stirred overnight at room temperature. Concentrated *in vacuo*. Employed immediately for alkyne azide cycloaddition reaction.

^{1}H NMR (D_2O, 300 Hz) δ_{ppm} : 4.48 (1H, d, J = 7.7 Hz, CH, H^3), 4.40 (2H, t, J = 2.2 Hz, CH_2-C≡CH, H^{2a+b}), 3.84 (1H, d, J=3.4 Hz, CH, H^5), 3.68 (2H, d, J = 3.0 Hz, CH_2 H^{8a+b}), 3.65 (1H, d, J = 2.6, CH, H^6) 3.60 (1H, t, J = 3.9, CH, H^5), 3.45 (1H, m, CH, H^7), 2.82 (1H, t, J = 2.4, C≡C*H*, H^1)

^{13}C NMR (D_2O, 100 Hz) δ_{ppm}: 101.0 (CH, C^4), 76.13 (CH_2-C≡*C*H, C^1), 75.20 (CH_2-*C*≡CH, C^2), 72.65 (CH, C^8), 71.1 (CH, C^6), 70.45 (CH, C^5), 68.51 CH, C^7), 60.68(CH_2 C^9), 56.0(CH_2-C≡CH, C^3)

Copper-catalyzed [3+2] cycloaddition of propargyl-pyrannosides and azide-$(PEG)_{3K}$-SH

N_3-$(PEG)_{3K}$-SH (20 mg, 5.9 μmol), (50 mg, 0.23 mmol), TEA (10 mg, 0.072 mmol), and CuBr (2 mg) dissolved in DMSO (4 mL) were charged in an ampoule and deoxygenated through three freeze–pump–thaw cycles before being placed under nitrogen. TBTA (8 mg, 0.14 mmol) was added and the reaction was degassed and left under nitrogen for 48 h. The polymer was purified by dialysis against water using dialysis tubing with MWCO of 1000 $g.mol^{-1}$.

IR ν : 3600-3200 (OH), 2890 (CH_2), 1105 (C-O) cm^{-1},

Preparation of Pyrannoside-$(PEG)_{3K}$ functionalised gold nanoparticles

To 5 mL of 40 nm AuNPs, pyrannoside-$(PEG)_{3K}$-SH (5 mg) was added and left for 30 mins at room temperature. The particles were then centrifuged at 6000 rpm for 15 mins and resuspended in HEPES buffer.

Analytical Measurements

Size Characterisation of Glucose Functionalized Gold Nanoparticles using Absorbance Spectra

50 μL of each glycoAuNP were loaded into a 96-well microtitre plate, 50 μL of 10 mM HEPES buffer with 0.5 mM $CaCl_2$, 0.5 mM $MnCl_2$ and 0.5 mM $MgCl_2$ was added to each and a spectrum was taken between 450 nm and 700 nm.

Concanavalin A Induced Aggregation Assays

A stock of 24 μg/mL Con A was made up in 10 mM HEPES buffer with 0.5 mM $CaCl_2$, 0.5 mM $MnCl_2$ and 0.5 mM $MgCl_2$. 50μL serial dilutions of ConA were made up in the same buffer in a 96-well microtitre plate so that when the nanoparticles were added the resultant concentration was 12nM – 0.01 nM and a control with 0 μg/mL of ConA. 50 μL of the glycoAuNP was added to each concentration of ConA and incubated at 37 °C for 30 minutes with medium shaking and then an absorbance spectra between 450 nm and 700 nm was recorded. Each measurement was done in triplicate.

Concanavalin A Induced Aggregation Kinetics Studies using Absorbance Spectra

50 μL of the nanoparticle solution was incubated with 50 μL of Con A at the K_d concentration. Readings of the absorbance at 700 nm were taken every minute for 30 seconds with medium shaking between recordings.

Concanavalin A Induced Aggregation Kinetics Studies using Dynamic Light Scattering

300 μL of AuNP was made up in 240 μL of MilliQ water and filtered through a 0.22 μm syringe filter. 60 μL of ConA was added that would make the concentration of ConA around the K_d value. Average diameter measurements at ambient temperature were taken every 15 seconds for 30 minutes.

Bacterial Detection Assay

An adapted procedure was used of that conducted by Seeberger *et al*.[4] TOP10 (nonfimbriated) and K-12 (fimbriated) *Escherichia coli* cells were cultured overnight in LB media at 37 °C. The culture was then washed twice and resuspended in HEPES buffer with 0.5 mM $CaCl_2$, 0.5 mM $MnCl_2$ and 0.5 mM $MgCl_2$. 100 μL serial dilutions of the bugs were made up in microtitre plates and 100 μL of the gold nanoparticles were added to the cells. The suspensions were incubated at room temperature for 30 minutes. The absorbance spectra of the nanoparticle cell suspensions were taken using the cells alone as a background. Colony forming units were estimated, assuming that OD_{600nm} 1 = 10^9 CFU.mL^{-1}.

References

1. D. J. Payne, M. N. Gwynn, D. J. Holmes and D. L. Pompliano, *Nat. Rev. Drug Discov.*, 2007, **6**, 29-40.
2. V. Makarov, G. Manina, K. Mikusova, U. Möllmann, O. Ryabova, B. Saint-Joanis, N. Dhar, M. R. Pasca, S. Buroni, A. P. Lucarelli, A. Milano, E. De Rossi, M. Belanova, A. Bobovska, P. Dianiskova, J. Kordulakova, C. Sala, E. Fullam, P. Schneider, J. D. McKinney, P. Brodin, T. Christophe, S. Waddell, P. Butcher, J. Albrethsen, I. Rosenkrands, R. Brosch, V. Nandi, S. Bharath, S. Gaonkar, R. K. Shandil, V. Balasubramanian, T. Balganesh, S. Tyagi, J. Grosset, G. Riccardi and S. T. Cole, *Science*, 2009, **324**, 801-804.
3. D. Pissuwan, C. H. Cortie, S. M. Valenzuela and M. B. Cortie, *Trends Biotech.*, 2010, **28**, 207-213.
4. M. D. Disney, J. Zheng, T. M. Swager and P. H. Seeberger, *J. Am. Chem. Soc.*, 2004, **126**, 13343-13346.
5. J. Joo, C. Yim, D. Kwon, J. Lee, H. H. Shin, H. J. Cha and S. Jeon, *Analyst*, 2012, **137**, 3609-3612.
6. K. Aslan, J. Zhang, J. R. Lakowicz and C. D. Geddes, *J. Fluoresence*, 2004, **14**, 391-400.
7. J. E. Ghadiali and M. M. Stevens, *Adv. Mater.*, 2008, **20**, 4359-4363.
8. S. Watanabe, K. Yoshida, K. Shinkawa, D. Kumagawa and H. Seguchi, *Colloids and Surfaces B-Biointerfaces*, 2010, **81**, 570-577.
9. C. L. Schofield, B. Mukhopadhyay, S. M. Hardy, M. B. McDonnell, R. A. Field and D. A. Russell, *Analyst*, 2008, **133**, 626-634.
10. Y. J. Chuang, X. C. Zhou, Z. W. Pan and C. Turchi, *Biochem. Biophys. Res. Commun.*, 2009, **389**, 22-27.

11. A. Laromaine, L. L. Koh, M. Murugesan, R. V. Ulijn and M. M. Stevens, *J. Am. Chem. Soc.*, 2007, **129**, 4156-+.

12. G. J. Nusz, S. M. Marinakos, A. C. Curry, A. Dahlin, F. Hook, A. Wax and A. Chilkoti, *Anal. Chem.*, 2008, **80**, 984-989.

13. A. K. Singh, D. Senapati, S. G. Wang, J. Griffin, A. Neely, P. Candice, K. M. Naylor, B. Varisli, J. R. Kalluri and P. C. Ray, *Acs Nano*, 2009, **3**, 1906-1912.

14. K. M. Mayer, S. Lee, H. Liao, B. C. Rostro, A. Fuentes, P. T. Scully, C. L. Nehl and J. H. Hafner, *Acs Nano*, 2008, **2**, 687-692.

15. S. H. Huang, *Sensor. Actuat. B-Chem*, 2007, **127**, 335-340.

16. A. J. Haes, L. Chang, W. L. Klein and R. P. Van Duyne, *J. Am. Chem. Soc.*, 2005, **127**, 2264-2271.

17. P. Englebienne, *Analyst*, 1998, **123**, 1599-1603.

18. N. Ohtake, K. Niikura, T. Suzuki, K. Nagakawa, H. Sawa and K. Ijiro, *Biocong. Chem.* , 2008, **19**, 507-515.

19. P. V. Baptista, M. Koziol-Montewka, J. Paluch-Oles, G. Doria and R. Franco, *Clin. Chem.*, 2006, **52**, 1433-1434.

20. R. Elghanian, J. J. Storhoff, R. C. Mucic, R. L. Letsinger and C. A. Mirkin, *Science*, 1997, **277**, 1078-1081.

21. R. de la Rica and M. M. Stevens, *Nat. Nano.*, 2012, **7**, 821-824.

22. O. R. Miranda, X. Li, L. Garcia-Gonzalez, Z.-J. Zhu, B. Yan, U. H. F. Bunz and V. M. Rotello, *J. Am. Chem. Soc.*, 2011, **133**, 9650-9653.

23. C. R. Bertozzi and L. L. Kiessling, *Science*, 2001, **291**, 2357-2364.

24. L. L. Kiessling, J. E. Gestwicki and L. E. Strong, *Angew. Chem. Int. Ed.*, 2006, **45**, 2348-2368.

25. M. Ambrosi, N. R. Cameron and B. G. Davis, *Org. Biomol. Chem*, 2005, **3**, 1593-1608.

26. H. Feinberg, D. A. Mitchell, K. Drickamer and W. I. Weis, *Science*, 2001, **294**, 2163-2166.

27. Y. C. Lee, R. R. Townsend, M. R. Hardy, J. Lonngren, J. Arnarp, M. Haraldsson and H. Lonn, *J. Biol. Chem.*, 1983, **258**, 199-202.

28. J. J. Lundquist and E. J. Toone, *Chem. Rev.*, 2002, **102**, 555-578.

29. S. Watanabe, H. Seguchi, K. Yoshida, K. Kifune, T. Tadaki and H. Shiozaki, *Tet. Lett.*, 2005, **46**, 8827-8829.

30. C. S. Tsai, T. B. Yu and C. T. Chen, *Chem. Commun.*, 2005, 4273-4275.

31. C. C. Lin, Y. C. Yeh, C. Y. Yang, G. F. Chen, Y. C. Chen, Y. C. Wu and C. C. Chen, *Chem. Commun.*, 2003, 2920-2921.

32. C. C. Lin, Y. C. Yeh, C. Y. Yang, C. L. Chen, G. F. Chen, C. C. Chen and Y. C. Wu, *J. Am. Chem. Soc.*, 2002, **124**, 3508-3509.

33. J. M. De la Fuente and S. Penades, *BioChem. Biophys. Acta*, 2006, **1760**, 636-651.

34. M. Hartmann and T. K. Lindhorst, *Eur. J. Org. Chem.*, 2011, 3583-3609.

35. G. Pasparakis, A. Cockayne and C. Alexander, *J. Am. Chem. Soc.*, 2007, **129**, 11014 - 11015.

36. M. J. Marin, A. Rashid, M. Rejzek, S. A. Fairhurst, S. A. Wharton, S. R. Martin, J. W. McCauley, T. Wileman, R. A. Field and D. A. Russell, *Org. Biomol. Chem*, 2013, **11**, 7101-7107.

37. W. Haiss, N. T. K. Thanh, J. Aveyard and D. G. Fernig, *Anal. Chem.*, 2007, **79**, 4215-4221.

38. R. J. Pieters, *Org. Biomol. Chem*, 2009, **7**, 2013-2025.

39. Y. Gou, S.-J. Richards, D. M. Haddleton and M. I. Gibson, *Polym. Chem.*, 2012, **3**, 1634-1640.

40. H. Otsuka, Y. Nagasaki and K. Kataoka, *Adv. Drug Del. Rev.*, 2003, **55**, 403-419.

41. T. R. Chan, R. Hilgraf, K. B. Sharpless and V. V. Fokin, *Org. Lett.*, 2004, **6**, 2853-2855.

Table of Contents Graphic

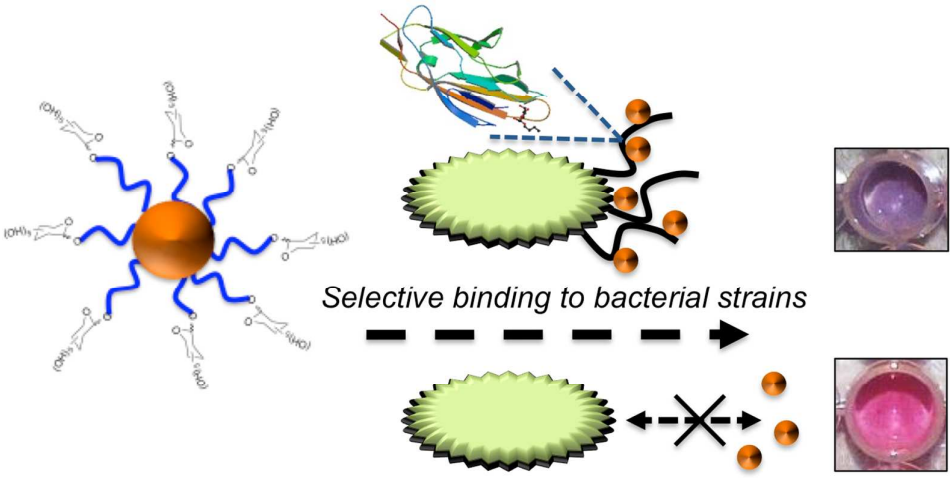

Table of Contents Text

Gold nanoparticles are employed to discriminate between bacterial strains based on their differential expression of carbohydrate-binding proteins. The role of carbohydrate presentation on sensory output is studied.